Wideband Chiral Metamaterial for Polarization Conversion Based on Helical-Type Inclusions

Ángel J. García-Collado, Gregorio J. Molina-Cuberos, Óscar Fernández Fernández, Ismael Barba, and José Margineda, *Life Member, IEEE*

***Abstract*— Materials with a high electromagnetic activity usually present a strong resonant response that produces extreme values for the constitutive parameters, but in a narrow frequency range. Here, a chiral material composed by four helical-like resonators, as the unit cell, able to produce high rotatory dispersion and low circular dichroism in a wide frequency band is presented. The transmission and reflection coefficients of a thin slab of such material have been determined using a free-wave experimental setup and numerical simulations. The experimental results show a cross-polarization conversion in the transmission mode for linearly polarized incident waves in a 2-GHz bandwidth centered at 10 GHz and a polarization conversion ratio larger than 0.97.**

***Index Terms*— Chirality, metamaterial (MM), polarization.**

I. Introduction

METAMATERIALS (MMs) have been proposed for cross-polarization converters in transmission [1], [2], [3], [4], [5], [6], [7], [8], [9], [10], [11], [12], [13] and reflection mode [14], [15], [16], [17]. Reflection-based converters are easier to design [11] and generally offer higher efficiency and broader bandwidths. However, the interference between incident and reflected waves can reduce the output signal quality [2], [3]. To achieve high transmission converter efficiency, multilayer structures combining several metal layers separated by dielectric material are typically used [12], [13], but this comes with the drawback of increased thickness.

Chiral media (CMs) are a specific type of MMs that affect the transmitted wave's polarization [18] and are proposed for cross-polarization converters in the transmission mode [5], [6], [7], [8], [9], [10]. CMs with non-C_4 symmetric unit cells achieve high transmission efficiency with 90° polarization conversion [5], [6], [7]. However, they are limited to either x- or y-polarized waves due to unit cell asymmetry. In contrast, C_4 symmetric structures present a polarization-insensitive response, providing cross-polarization for both the x- and y-polarized waves. However, they provide very narrow frequency bands [8], [9], [10]. For instance, [8] found a 0.2-GHz bandwidth at ∼12.9 GHz, and [9] identified a 0.4-GHz bandwidth at ∼16.8 GHz. In some cases [10], the presence of several resonances generates multiple frequencies with polarization conversion, albeit with significantly narrower bandwidths.

Here, we introduce a novel CM for transmission mode cross-polarization applications in the microwave frequency range. Four helical-type resonators with the same handedness are properly twisted to achieve C_4 symmetry for incident waves perpendicular to the surface. The resulting response remains independent of the incident wave's polarization direction, providing a 90° polarization rotation within a 2-GHz bandwidth. This bandwidth exceeds that of other C_4 symmetric CMs operating in the transmission mode [8], [9], [10].

II. Characterization

CMs can be macroscopically described by including the parameter κ into the constitutive equations to quantify the electromagnetic coupling [18]

$$\vec{D} = \epsilon_0 \epsilon_r \vec{E} - i\sqrt{\epsilon_0 \mu_0}\kappa \vec{H} \quad (1)$$

$$\vec{B} = \mu_0 \mu_r \vec{H} + i\sqrt{\epsilon_0 \mu_0}\kappa \vec{E} \quad (2)$$

where ϵ_r is the relative dielectric permittivity, μ_r is the relative magnetic permeability, and κ is the chirality parameter.

Fig. 1 shows the experimental setup and the unit cell that is built on a standard FR4 board ($\epsilon_r = 4.2$, $\tan\delta = 0.014$, and copper metallization thickness of 35 μm). A split ring is etched on each face of the PCB and interconnected through vias to create a helix-like structure of 35-mm length. The unit cell is 13.2 × 13.2 mm, and the sample is formed by 16 × 21 unit cells with a total surface of 580 cm^2. The dimensions of the structure were designed to maximize the response and to keep the effects into the experimental frequency band (7–15 GHz).

The sample was characterized using a free-space technique [19]. An ellipsoidal mirror focuses the incident beam to decrease diffraction problems [20]. Mismatches from the antennas, remaining edge diffraction effects, and unwanted reflections are filtered out using time-domain transforms.

To verify the experimental results, simulations using a commercially available electromagnetic simulator, CST Studio Suite, have been developed. An infinite slab was simulated by modeling a single unit cell with periodic boundary conditions.

Manuscript received 1 August 2023; accepted 4 September 2023. This work was supported by the Spanish Project through the European Commission (ERDF) under Grant PGC2018-098350-B-C21 and Grant PGC2018-098350-B-C22. *(Corresponding author: Gregorio J. Molina-Cuberos.)*

Ángel J. García-Collado is with the Departamento Ciencias Politécnicas. GRITA, Universidad Católica de Murcia, 30107 Murcia, Spain (e-mail: ajgarcia@ucam.edu).

Gregorio J. Molina-Cuberos and José Margineda are with the Departamento Electromagnetismo y Electrónica, Universidad de Murcia, 30100 Murcia, Spain (e-mail: gregomc@um.es; jmargi@um.es).

Óscar Fernández Fernández is with the Departamento de Ingeniería de Comunicaciones, Universidad de Cantabria, 39005 Santander, Spain (e-mail: oscar.fernandez@unican.es).

Ismael Barba is with the Departamento de Electricidad y Electrónica, Universidad de Valladolid, 47002 Valladolid, Spain (e-mail: ismael.barba@uva.es).

Color versions of one or more figures in this letter are available at https://doi.org/10.1109/LMWT.2023.3313644.

Digital Object Identifier 10.1109/LMWT.2023.3313644

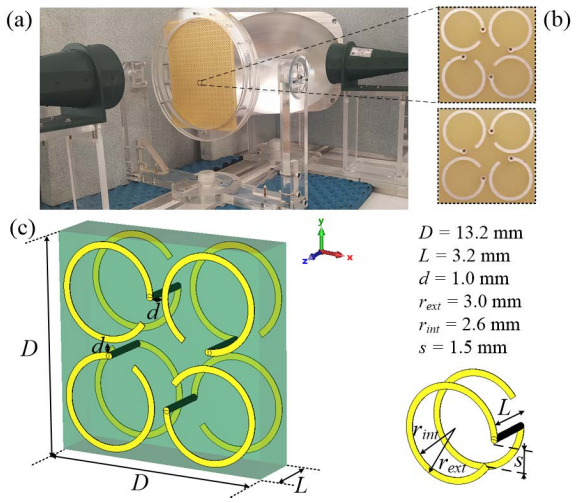

Fig. 1. (a) Photograph of the experimental set up. (b) Detail of front (upper) and back (lower) metallic layers. (c) Diagram of the unit cell (left) composed by four structures (right).

The transmitted wave for CMs is usually described in terms of the transmission coefficients for the right- and left-handed circularly polarized waves, T_{++} and T_{--}. These coefficients are related to the linear ones by $T_{++} = T_{yy} + iT_{xy}$ and $T_{--} = T_{yy} - iT_{xy}$ for a y-polarized incident wave, where T_{yy} and T_{xy} are the transmission coefficients for the copolar and crosspolar waves, respectively. Owing to the C_4 symmetry of the CM, the response is independent of the polarization direction, i.e., $T_{xx} = T_{yy}$, $T_{xy} = -T_{yx}$, $R_{xx} = R_{yy}$, and $R_{xy} = R_{yx} = 0$.

The angle between the polarization of the incident wave and the semi major axis of the elliptically polarized transmitted wave, θ, the ellipticity of the transmitted wave, η, and the chirality parameter, κ, are obtained from [21]

$$\theta = \frac{1}{2}\arg\left(\frac{T_{++}}{T_{--}}\right) \tag{3}$$

$$\eta = \frac{1}{2}\tan^{-1}\left(\frac{|T_{++}|^2 - |T_{--}|^2}{|T_{++}|^2 + |T_{--}|^2}\right) \tag{4}$$

$$\kappa = -\frac{i}{2k_0 L}\ln\left|\frac{T_{++}}{T_{--}}\right| + \frac{1}{2k_0 L}\arg\left(\frac{T_{++}}{T_{--}}\right) + \frac{2\pi p}{k_0 L} \tag{5}$$

where $k_0 = \omega(\epsilon_0\epsilon_r\mu_0\mu_r)^{1/2}$, p is an integer that is obtained by considering that far from the resonance $p = 0$, and $\mathrm{Im}(\kappa) = 0$. It is also necessary that $\mathrm{Re}(\kappa)$ and $\mathrm{Im}(\kappa)$ fulfill the Kramers–Kronig relations [22].

III. Results and Discussion

Fig. 2 shows transmission and reflection coefficients from the experimental data and numerical simulations. We find three resonances in the experimental frequency band: 8.90, 11.30, and 13.90 GHz. Simulations confirm these resonances and show two more resonances at frequencies below the experimental band: 2.42 and 4.86 GHz, not shown for clarity. For frequencies larger than 8.90 GHz, we observe that $|T_{xy}| > |T_{yy}|$. At 11.30 GHz, the ratio $|T_{xy}|/|T_{yy}|$ reaches the maximum, and for $f > 11.30$ GHz, this ratio decreases to reach the unity at 13.90 GHz. Therefore, $|T_{xy}| > |T_{yy}|$ between 8.90 and 13.90 GHz, which means that the amplitude of the crosspolar transmitted field is larger than the copolar one.

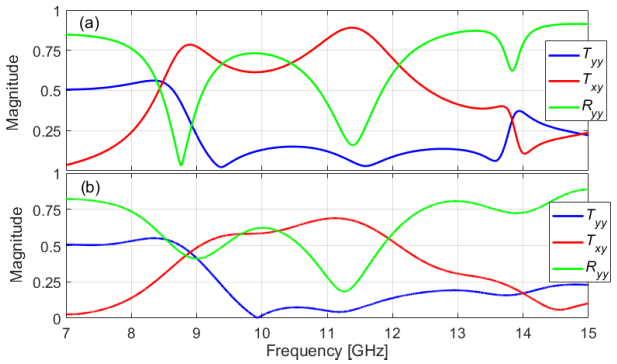

Fig. 2. Transmission (T_{yy}, T_{xy}) and reflection (R_{yy}) coefficients obtained from (a) simulation and (b) experiments.

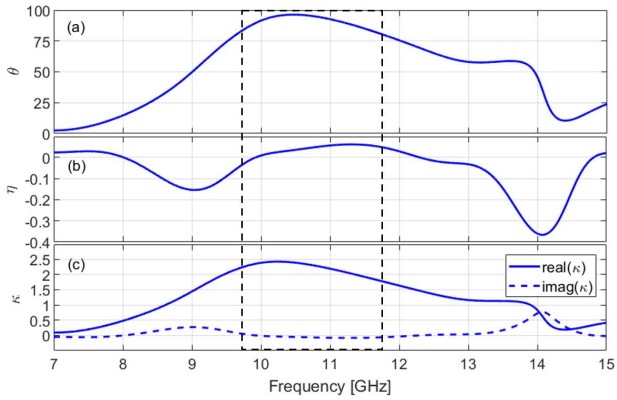

Fig. 3. (a) Retrieved rotation angle, (b) ellipticity, and (c) chirality obtained from the experimental data. The dotted black line shows the frequency band for 90° polarization rotation.

Fig. 3 shows the retrieved values for θ, η, and κ. Between 8.90 and 13.90 GHz, $\theta > 45°$, and η is in the range from -0.35 to 0.05 rad, being maximum (in absolute value) at the edges of the band. Furthermore, between 9.65 and 11.75 GHz, $\theta = 90° \pm 10\%$ and η is found to be very low, $|\eta| < 0.05$ rad. Therefore, this CM works as a linear polarization converter, providing a rotation of 90° without polarization distortion in a relative bandwidth ($\delta f/f_{\mathrm{mean}}$) of 20% and with a polarization conversion ratio [PCR $= |T_{xy}|^2/(|T_{xy}|^2 + |T_{yy}|^2)$] larger than 0.97. It is important to highlight that this conversion is independent of the incident polarization (x- or y-polarized) due to the C_4 symmetry of the structure.

The chirality parameter resonates at 8.90 and 13.90 GHz, where $\mathrm{Im}(\kappa)$ reaches local extremes. However, the frequency dependence at the resonances does not follow a single-frequency Condon model [23] as it has been widely found in the literature [24], [25], [26], [27]. In a typical Condon behavior, $\mathrm{Re}(\kappa)$ changes its sign and $\mathrm{Im}(\kappa)$ peaks at the resonance frequency, and both the real and imaginary parts tend to zero far from the resonance. However, we have not found such change on the sign of $\mathrm{Re}(\kappa)$ at the resonance. The obtained value for $\mathrm{Re}(\kappa)$ increases with the frequency below and above 8.90 GHz and it reaches a maximum of around 2.5 at 10.25 GHz. Then, $\mathrm{Re}(\kappa)$ decreases with frequency and at 13.90 GHz $\mathrm{Im}(\kappa)$ reaches a maximum, which shows the presence of a resonant frequency.

Fig. 4 shows the polarization ellipse of the incident and transmitted signals for eight selected frequencies. The transmitted wave is linear for most of the frequencies,

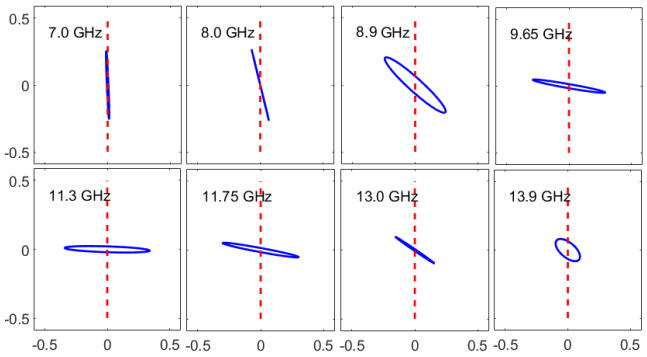

Fig. 4. Polarization ellipse of the transmitted (blue solid line) and incident waves (red dashed line) for selected frequencies.

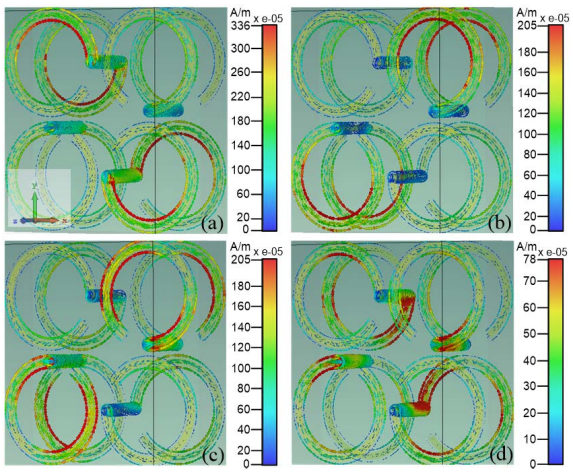

Fig. 5. Current distribution at the four first resonance frequencies. (a) 2.4 GHz, (b) 4.9 GHz, (c) 8.9 GHz, and (d) 11.3 GHz. In every case, the phase is such that the current is maximum [270° in (a) and (b), and 180° in (c) and (d)].

except at the resonances 8.90 and 13.90 GHz, where η presents local extremes. The rotation angle θ varies from 0° (y-polarized) outside the band without chiral behavior to 45° at the resonances, reaching ≈90° (x-polarized) in the 9.65–11.75-GHz band. In this band, the metasurface behaves as a linear polarization converter with a low distortion of the polarization. For $f > 13$ GHz, the magnitude of the transmitted signal decreases because most of the signal is reflected; see Fig. 2.

The polarization ellipse for the minimum and maximum frequencies of the 90° polarization conversion band, 9.65 and 11.75 GHz, is also shown. These two cases present a rotation angle of 81° and an ellipticity of −0.05 rad.

Fig. 5 shows the current distribution at the first four resonances, which correspond to different excited modes. The 2.4- and 4.9-GHz resonances are outside of the experimental frequency range, they were detected in simulations, and they displayed for a better illustration of the current modes.

The first mode, at 2.4 GHz, shows a current maximum in the center of the helix and nulls in its edges. Meanwhile, for the second resonance, at 4.9 GHz, the current is null in the center and the edges of the helix and has two maximums (with opposite current direction). Both correspond to the first and second harmonics of a 35-mm length helix [28]. The 8.9-GHz resonance is similar to the third harmonic, although the neighboring helices produce some perturbations. However, 11.3 GHz is so affected by the neighboring helices that its

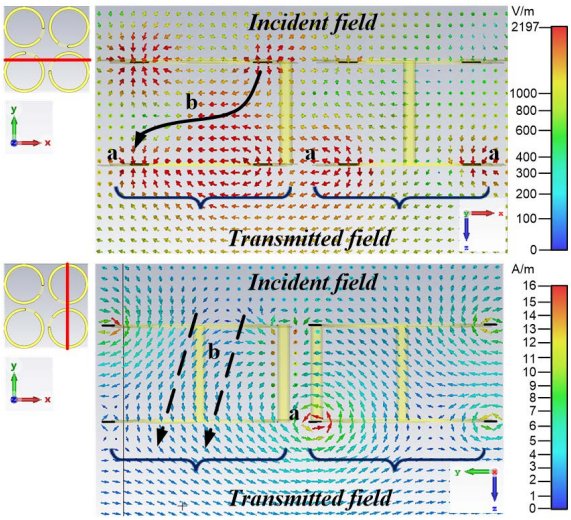

Fig. 6. Electric and magnetic fields at 9.9 GHz and phase 270°, in the area inside the structure (cut marked in the left figure). The coupling between neighboring helices is marked with an "a" while the distribution of the electric/magnetic field between both the edges of each helices is shown in "b."

correspondence with a specific harmonic is not so clear. In fact, the location of this resonance strongly depends on the distance between the helices.

Previously, a single helical-type resonator lacking C4 symmetry was used to generate passbands for x-to-y and y-to-x polarization conversion [7]. In contrast, our proposed structure of four resonators introduces three resonances at 8.9, 11.3, and 13.9 GHz, resulting in a broader conversion band for both the x- and y-polarized incident waves compared with [7].

Fig. 6 shows the field structure at 9.9 GHz, an arbitrary frequency between 9.65 and 11.75 GHz. We see the typical response of a helical resonator that produces the electromagnetic activity [28]. The electric field between the edges of the helix generates a current and, then, a magnetic dipole inside the structure (dashed black arrow, bottom plot). Therefore, the incident y-polarized electric field is converted into x polarization after transmission. And vice versa, a magnetic field inside the structure induces an electric current that leads to a potential difference between the edges of the helix (solid-black arrow, top plot). There is also a clear electromagnetic coupling between neighboring helices, so they cannot be treated as isolated resonators. Our simulations show that the rotation bandwidth depends on the geometric parameters of the whole unit cell, mainly on the distance between the neighboring helices, and not only on the individual helix dimensions.

IV. Conclusion

Here, an MM based on a chiral structure with C_4 symmetry has been presented. This structure, which operates in the transmission mode, exhibits a 90° polarization rotation with low dispersion over a wide frequency band, from 9.65 to 11.75 GHz. The PCR is higher than 0.97 in all the bands, providing a linear crosspolar transmitted field with very low ellipticity, i.e., low distortion.

References

[1] W. Liu et al., "Realization of broadband cross-polarization conversion in transmission mode in the terahertz region using a single-layer metasurface," *Opt. Lett.*, vol. 40, no. 13, p. 3185, 2015.

[2] N. K. Grady et al., "Terahertz metamaterials for linear polarization conversion and anomalous refraction," *Science*, vol. 340, no. 6138, pp. 1304–1307, Jun. 2013.

[3] L. Cong et al., "A perfect metamaterial polarization rotator," *Appl. Phys. Lett.*, vol. 103, no. 17, Oct. 2013.

[4] X. Jing, X. Gui, P. Zhou, and Z. Hong, "Physical explanation of Fabry–Pérot cavity for broadband bilayer metamaterials polarization converter," *J. Lightw. Technol.*, vol. 36, no. 12, pp. 2322–2327, Jun. 15, 2018.

[5] J. Shi et al., "Dual-band asymmetric transmission of linear polarization in bilayered chiral metamaterial," *Appl. Phys. Lett.*, vol. 102, no. 19, May 2013.

[6] C. Huang, X. Ma, M. Pu, G. Yi, Y. Wang, and X. Luo, "Dual-band 90° polarization rotator using twisted split ring resonators array," *Opt. Commun.*, vol. 291, pp. 345–348, Mar. 2013.

[7] L. Wu, M. Zhang, B. Zhu, J. Zhao, T. Jiang, and Y. Feng, "Dual-band asymmetric electromagnetic wave transmission for dual polarizations in chiral metamaterial structure," *Appl. Phys. B, Lasers Opt.*, vol. 117, no. 2, pp. 527–531, Nov. 2014.

[8] R. Rajkumar, N. Yogesh, and V. Subramanian, "Cross polarization converter formed by rotated-arm-square chiral metamaterial," *J. Appl. Phys.*, vol. 114, no. 22, Dec. 2013.

[9] L. Wang, F. Lv, Z. Xiao, and X. Ma, "Theoretical and experimental verification of 90° polarization converter based on chiral metamaterials," *Plasmonics*, vol. 16, no. 1, pp. 199–204, Feb. 2021.

[10] H.-Y. Shi, J.-X. Li, A.-X. Zhang, J.-F. Wang, and Z. Xu, "Tri-band transparent cross-polarization converters using a chiral metasurface," *Chin. Phys. B*, vol. 23, no. 11, Nov. 2014, Art. no. 118101.

[11] F. A. Dicandia and S. Genovesi, "Design of a transmission-type polarization-insensitive and angularly stable polarization rotator by using characteristic modes theory," *IEEE Trans. Antennas Propag.*, vol. 71, no. 2, pp. 1602–1612, Feb. 2023.

[12] D.-J. Liu, Z.-Y. Xiao, X.-L. Ma, and Z.-H. Wang, "Broadband asymmetric transmission and multi-band 90° polarization rotator of linearly polarized wave based on multi-layered metamaterial," *Opt. Commun.*, vol. 354, pp. 272–276, Nov. 2015.

[13] W. Hong, J. Zhu, L. Deng, L. Wang, and S. Li, "Perfect terahertz-wave polarization rotator using dual Fabry–Perot-like cavity resonance metamaterial," *Appl. Phys. A, Solids Surf.*, vol. 125, no. 8, pp. 1–7, Aug. 2019.

[14] J. Zhu, S. Li, L. Deng, C. Zhang, Y. Yang, and H. Zhu, "Broadband tunable terahertz polarization converter based on a sinusoidally-slotted graphene metamaterial," *Opt. Mater. Exp.*, vol. 8, no. 5, pp. 1164–1173, May 2018.

[15] Q. Zheng, C. Guo, and J. Ding, "Wideband metasurface-based reflective polarization converter for linear-to-linear and linear-to-circular polarization conversion," *IEEE Antennas Wireless Propag. Lett.*, vol. 17, no. 8, pp. 1459–1463, Aug. 2018.

[16] R. Lin et al., "Multiple interference theoretical model for graphene metamaterial-based tunable broadband terahertz linear polarization converter design and optimization," *Opt. Exp.*, vol. 29, no. 19, pp. 30357–30370, 2021.

[17] F. Ding, Z. Wang, S. He, V. M. Shalaev, and A. V. Kildishev, "Broadband high-efficiency half-wave plate: A supercell-based plasmonic metasurface approach," *ACS Nano*, vol. 9, no. 4, pp. 4111–4119, Apr. 2015.

[18] I. V. Lindell, A. H. Sihvola, S. A. Tretyakov, and A. J. Viitanen, *Electromagnetic Waves in Chiral and Bi-Isotropic Media*. Boston, MA, USA: Artech House, 1994.

[19] J. Margineda, G. J. Molina-Cuberos, M. Núñez, A. J. García-Collado, and E. Martín, "Electromagnetic characterization of chiral media," in *Solutions and Applications of Scattering, Propagation, Radiation and Emission of Electromagnetic Waves*. London, U.K.: Intech, 2012.

[20] M. Rojo, J. Muñoz, G. J. Molina-Cuberos, Á. J. García-Collado, and J. Margineda, "Design of an ellipsoidal mirror for freewave characterization of materials at microwave frequencies," *Meas. Sci. Technol.*, vol. 27, no. 3, Mar. 2016, Art. no. 035001.

[21] R. Zhao, T. Koschny, and C. M. Soukoulis, "Chiral metamaterials: Retrieval of the effective parameters with and without substrate," *Opt. Exp.*, vol. 18, no. 14, p. 14553, 2010.

[22] F. Guérin and A. Lakhtakia, "On the frequency-dependence of the chirality pseudoscalar of a chiral medium," *J. de Phys. III*, vol. 5, no. 7, pp. 913–918, Jul. 1995.

[23] E. U. Condon, "Theories of optical rotatory power," *Rev. Modern Phys.*, vol. 9, no. 4, pp. 432–457, Oct. 1937.

[24] E. Plum et al., "Metamaterial with negative index due to chirality," *Phys. Rev. B, Condens. Matter*, vol. 79, no. 3, Jan. 2009, Art. no. 035407.

[25] G. J. Molina-Cuberos, A. J. Garcia-Collado, J. Margineda, M. J. Nunez, and E. Martin, "Electromagnetic activity of chiral media based on Crank inclusions," *IEEE Microw. Wireless Compon. Lett.*, vol. 19, no. 5, pp. 278–280, May 2009.

[26] Z. Li et al., "Chiral metamaterials with negative refractive index based on four 'U' split ring resonators," *Appl. Phys. Lett.*, vol. 97, no. 8, Aug. 2010, Art. no. 081901.

[27] F. Bayatpur, S. Wheeland, A. V. Amirkhizi, and S. Nemat-Nasser, "A varactor-tuned helix-based chiral layer," *IEEE Microw. Wireless Compon. Lett.*, vol. 23, no. 5, pp. 246–248, May 2013.

[28] J. Antoniuk, M. Zukocinski, A. Abramowicz, and W. Gvvarek, "Resonant frequencies of helical resonators," in *Proc. 11th Microcoll*, Budapest, Hungary, 2003, pp. 1044–1046.